Developmental Biology 450 (2019) 1–8

Contents lists available at ScienceDirect

Developmental Biology

journal homepage: www.elsevier.com/locate/developmentalbiology

Short Communication

Multiplex clonal analysis in the chick embryo using retrovirally-mediated combinatorial labeling

Weiyi Tang, Yuwei Li, Shashank Gandhi, Marianne E. Bronner *

Division of Biology and Biological Engineering, California Institute of Technology, Pasadena, CA 91125, USA

ARTICLE INFO

Keywords:
Replication incompetent avian retrovirus
Multiplexed clonal analysis
Combinatorial labelling
Neural tube
Trunk neural crest
Multipotency

ABSTRACT

Lineage analysis plays a central role in exploring the developmental potential of stem and progenitor cell populations. In higher vertebrates, a variety of techniques have been used to label individual cells or cell populations, including interspecies grafting, intracellular microinjection, and Cre-mediated recombination. However, these approaches often suffer from difficulties in progenitor cell targeting, low cellular resolution and/or ectopic labeling. To circumvent these issues, here we utilize replication incompetent avian (RIA) retroviruses to deliver combinations of fluorescent proteins into distinct cellular compartments in chick embryos. In particular, RIA-mediated lineage tracing is optimal for long term mapping of dispersing cell populations like the neural crest. Using this tool, we confirm that trunk neural crest cells are multipotent. Furthermore, our RIA vector is engineered to be fully adaptable for other purposes such as cell fate analysis, gene perturbation studies and time-lapse imaging. Taken together, we present a novel approach of multiplex lineage analysis that can be applied to normal and perturbed development of diverse cell populations in avian embryos.

1. Introduction

A fundamental challenge in developmental biology is to determine the range of cell types that can arise from single embryonic cells. Whereas the fertilized egg or embryonic stem cells are totipotent, other embryonic cell types may be multipotent, bipotent or unipotent. Distinguishing between these possibilities requires methods that enable analysis of a cell's developmental history. In organisms like *C. elegans*, cell lineage analysis has been elegantly done by visually mapping the progeny of each cell division (Sulston, 1983). While this was a technical *tour de force* in a simple organism, it is not feasible in more complex and/or opaque organisms. Analysis of cell lineage is particularly challenging in vertebrate embryos.

In the past decades, various techniques have been developed to follow and analyze cell fates that greatly expanded our understanding of both embryogenesis and organogenesis. One approach is to directly inject single cells with fluorescent dyes that are large and thus cannot pass through gap junctions (Bronner-Fraser and Fraser, 1988). A second approach involves virally-mediated lineage analysis using β-galactosidase (Frank and Sanes, 1991; Sanes, 1989) or barcoded libraries (Gerrits et al., 2010). Third, quail-chick chimeric grafts have been a well-established tool for understanding the contribution of neural crest in avian embryos (Ayer-Le Lievre and Le Douarin, 1982). Finally, transgenic *Confetti* and Brainbow technology in mice and zebrafish, respectively, have been used to express fluorescent proteins at specific time points, enabling clonal analysis using high resolution imaging (Cai et al., 2013; Livet et al., 2007). A complication of the latter, however, is that it is difficult to establish clonality as it involves sophisticated statistical analysis of rare color combinations (Baggiolini et al., 2015). Moreover, this technology is not easily applicable to non-genetic organisms and is particularly challenging for cell types that are migratory and thus disperse widely in the embryo.

One example of such a cell type is the neural crest. Neural crest cells originate within the closing neural tube but then migrate to diverse locations in the embryo and form diverse cell types (Ayer-Le Lievre and Le Douarin, 1982). Despite the broad range of the neural crest derivatives at a population level, there are conflicting views in the literature regarding the degree of multipotency of individual neural crest cells. Single cell lineage analysis using microinjection of fluorescent dyes suggested that trunk neural crest cells in avian embryos are multipotent at both pre-migratory (Bronner-Fraser and Fraser, 1988) and migratory (Bronner--Fraser and Fraser, 1989) stages. In the mouse, Sommer and colleagues (Baggiolini et al., 2015) found similar results using *R26R-Confetti* technology. However, other studies have suggested that neural crest cells are

* Corresponding author.
E-mail address: mbronner@caltech.edu (M.E. Bronner).

https://doi.org/10.1016/j.ydbio.2019.03.007
Received 6 December 2018; Received in revised form 11 March 2019; Accepted 12 March 2019
Available online 15 March 2019

restricted in their fate, even before emigration from the neural tube (Krispin et al., 2010; Weston and Thiery, 2015). Thus, further analysis of neural crest lineage is warranted, particularly since little is known about their developmental potential at axial levels other than the trunk region.

The chick embryo has been an excellent system for neural crest biology. As amniotes, chick embryos develop similar to humans at stages of neural crest migration, but are cost-effective compared with mice. Moreover, their ability to develop outside of the mother facilitates not only genetic and surgical manipulations but also dynamic imaging (Bénazéraf et al., 2010). Recently, we have applied RIA-mediated lineage analysis to chick cartilage to understand how sister cells rearrange within a constrained region surrounded by extracellular matrix (Li et al., 2017). Here, we expand the repertoire of colors and subcellular localizations of these reagents and demonstrate their utility for defining clonal relationship of other cell types, including those that disperse widely in the embryo, like neural crest cells. As proof of principle, we confirm the multipotent property of trunk neural crest cells. Thus, our study enriches the toolkit for cell lineage analysis in a non-genetic model organism.

2. Materials and methods

2.1. Molecular cloning and virus preparation

The original RIA vector (Chen et al., 1999) was modified by inserting AscI, SpeI, NotI upstream of existing ClaI digestion site. H2B-YFP (#96893), H2B-RFP (#92398), Mito-CFP (#36208), Membrane-YFP (#56558) and Utrophin-Scarlet (#26739) were obtained from Addgene, and were subsequently subcloned into the modified RIA vector. ENV-A plasmid encoding the Envelope A protein was a gift from Dr. Connie Cepko and colleagues (Chen et al., 1999). ENV-A plasmid was co-transfected with recombinant RIA plasmids into chick DF1 cells to pseudotype RIA virus (ATCC, Manassas, VA; #CRL-12203, Lot number 62712171, Certificate of Analysis with negative mycoplasma testing available at ATCC website) in 15 cm culture dishes using standard transfection protocols. 24 h post-transfection, the cell culture medium was harvested twice per day for four days, and concentrated at 26, 000 rpm for 1.5 h. The pellet was dissolved in 20–30 μl of DMEM to achieve the titer of 1×10^7 pfu/ml. The viral aliquots were stored in −80 °C until injection.

2.2. Virus titering and clonal analysis in DF1 cells

Concentrated virus was serially diluted at $1{:}10^4$, $1{:}10^5$, $1{:}10^6$, and $1{:}10^7$ respectively, in 200 μl of DMEM. The diluted viral solution was added to chick DF1 cells in 24-well-plates. Cells were incubated at 38 °C for two hours to permit viral infection. Another 800 μl DMEM was subsequently added and infected cells were incubated for 72 h to allow for the expression of fluorescent proteins, which was used as a readout for functional recombinant virus. The number of cell clusters was quantified under an epifluorescence microscope. Typically, within a well of cells infected with the virus at $1{:}10^7$ dilution, one positive cluster was observed, meaning the viral titer is around 1×10^7 pfu/ml. For clonal analysis in DF1 cells, a mixture of H2B-RFP, Mem-YFP and Mito-CFP viruses was serially diluted and infected DF1 cells as above. The number of cell clusters (clones) with distinct color(s) in a given field of view (n = 3) was quantified using image software FIJI.

2.3. Viral injection and chick embryology

Equal amounts of RIA viruses encoding H2B-YFP, H2B-RFP, Mito-CFP, Membrane-YFP and Utrophin-Scarlet were mixed. A working solution was made at 1:2 dilution of the viral mixture with Ringer's solution (0.9% NaCl, 0.042%KCl, 0.016%$CaCl_2 \bullet 2H_2O$ wt/vol, pH7.0), and supplemented with 0.3 μl of 2% food dye (Spectral Colors, Food Blue 002, C.A.S# 3844-45-9) as an indicator. About 1 μl of working solution was injected into the lumen of the neural tube posterior to somite 3 in HH11 chicken embryos. The embryos were sealed with surgical tape, incubated at 37 °C for 2 days. Embryos were harvested at HH21 (n = 16), dissected and a 500 μm thick transverse slice at forelimb region was cut for imaging analysis (detailed procedure in Li et al., 2019). For immunohistochemistry, embryos were fixed in 4% PFA in PBS for 30 min at 4 °C, embedded in Tissue-Tek O.C.T compound (Sakura #4583) and sectioned (*Microm* HM550 cryostat).

2.4. Immunohistochemistry and imaging analysis

Frozen tissue sections were incubated in 1xPBS at room temperature to remove O.C.T, permeabilized with 0.3% vol/vol Triton-X100 in 1xPBS. Primary and secondary antibodies were diluted in blocking buffer (1xPBS with: 5% vol/vol normal donkey serum, 0.3% vol/vol Triton-X100). Sections were stained with primary antibody at 4 °C overnight (primary antibody dilutions: 1:500 Mouse anti-smooth muscle actin, Sigma-Cat# F1840-200μG; 1:500 Mouse antiHuC/D IgG2b, Invitrogen-Cat#A21271; 1:10 E1.9 primary sensory and motor neuron marker, DSHB). The next day, sections were washed with 1xPBS, and treated with secondary antibody for 1 h at room temperature. The following secondary antibodies were used: 1:1000 donkey anti-mouse IgG 647, 1:1000 goat anti-mouse IgM 647, 1:1000 goat anti mouse IgG2b 647, Molecular Probes. Sections were imaged using a Zeiss AxioImager.M2 with Apotome.2 and Zeiss LSM 800 confocal microscope. The number of infected cells displaying single color was quantified with thresholding followed by automated particle analysis using FIJI software. The number of doubly and triply infected cells was counted manually. For Feret's angle analysis of clonal orientation, a cell cluster with identical double-or triple-color was identified. Subsequently, a polygon was drawn along the boundary of the clone and the angle of the polygon was automatically measured by FIJI.

3. Results and discussion

3.1. Optimization and in vitro validation of replication-incompetent avian (RIA) retroviruses for multiplex clonal analysis

RIA retrovirus has been employed widely for lineage tracing in chick embryos (Chen et al., 1999). After stably integrating into host genome, RIA DNA is faithfully and equally passaged to daughter cells during cell division. In contrast to replication-competent avian (RCAS) virus (Fig. 1A), RIA does not synthesize its own envelope (ENV) protein and thus cannot horizontally transfer into neighboring cells. As a result, all descendants of an RIA infected cell are permanently labeled with a unique common signature, representing an isogenic clone. This feature offers several advantages over other approaches for lineage analysis: first, it is less invasive compared to quail-chick grafts, marking endogenous host cells without the necessity for surgery or combining tissue from different species; second, compared with progressively diluting vital dyes, the integrated RIA transgene enables indelible marking of host cells and their progeny (Li et al., 2018); finally, compared to *Confetti* mouse and zebrafish labeling, RIA ensures specific targeting of progenitor cells through focal injection, avoiding the general challenges faced by the Cre-lox systems that are dependent upon the choice of promoters (Lewis et al., 2013).

Previous studies have used RIA viruses to resolve clonal boundaries in cartilage, tendon, perichondrium and retina (Li et al., 2017; Pearse et al., 2007). One common characteristic of all these tissues is that they are comprised of coherent clones with regular morphology. To extend this analysis to broader types of tissues, we have optimized this approach and expanded its application to cells that migrate extensively and actively rearrange.

To this end, we modified the previous version of the RIA vector (Chen et al., 1999) by adding three unique restriction enzyme sites (AscI, SpeI, NotI) in the upstream of the common cloning site ClaI. The AscI and SpeI sites were preserved for expanding the application of this viral vector for

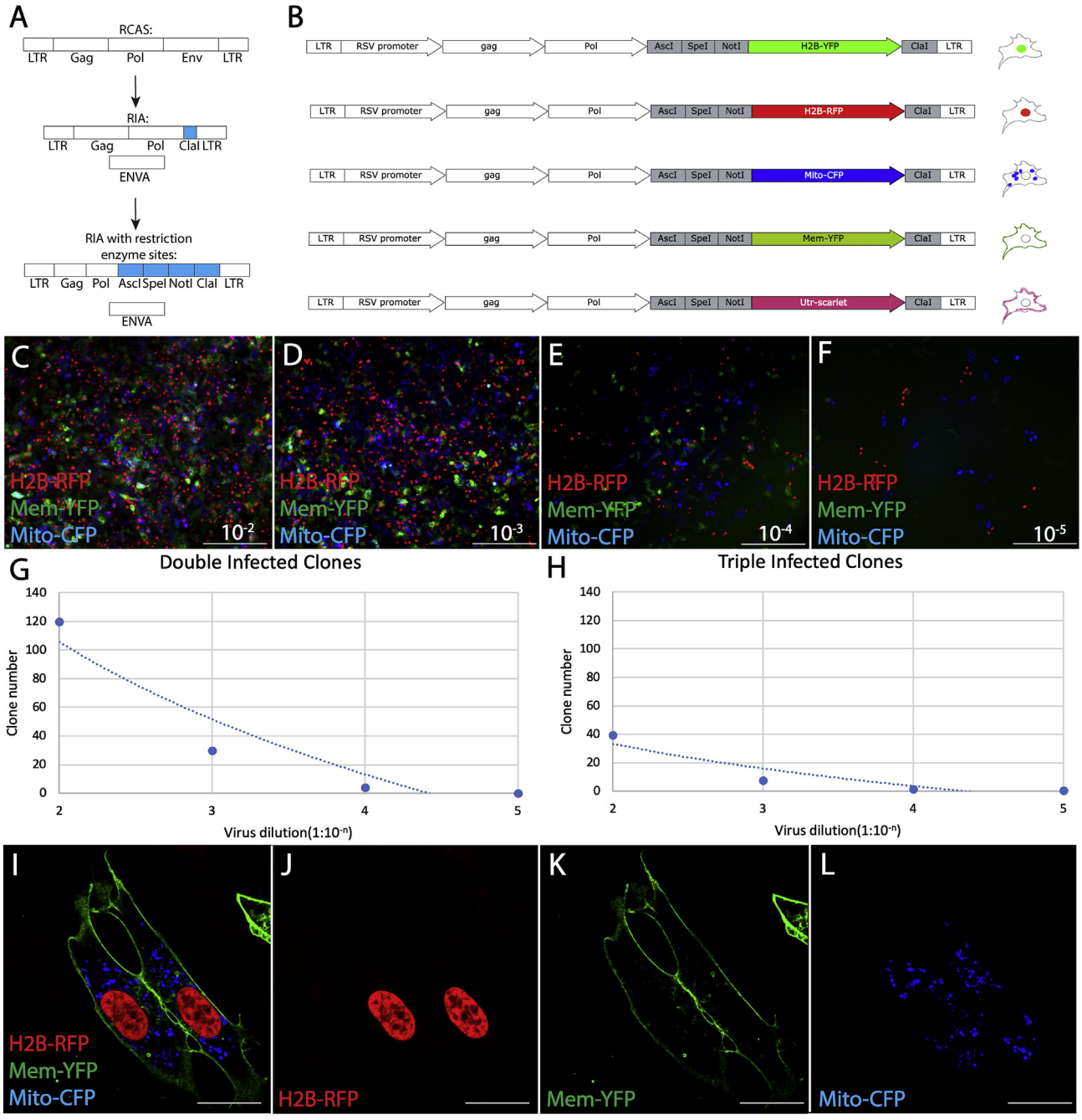

Fig. 1. Validating RIA-mediated multicolor clonal analysis in cell culture. (A) Construct map of RCAS, RIA, and modified RIA with restriction enzyme sites (blue). (B) Transgenes encoding fluorescent proteins targeted to specific subcellular regions were cloned into the RIA vector. Note the maps in (A) and (B) are not to scale. (C–F) Equal mixture of three viruses (H2B-RFP, Mem-YFP, Mito-CFP) was serially diluted and infected into DF1 cells. (G, H) The number of double and triple-infected clones showed an inverse relationship to viral titer. (I–L) High magnification imaging on infected cells with 63× objective lens confirmed specific subcellular targeting of fluorescent proteins. Scale bars: C-F 100 μm, I-L 10 μm.

future research, such as, creating fusion proteins and bicistronic systems to visualize protein dynamics and perform gene functional study, respectively. For the purpose of lineage tracing in wild-type chick embryos in this study, we generated five distinct viruses by inserting *H2B-YFP, H2B-RFP, Mito-CFP, Membrane-YFP (Mem-YFP), Utrophin-Scarlet (Utr-Scarlet)* between NotI and ClaI sites (Fig. 1B). Clonality assessment was based on three criteria: a complex color combination created by multiple (two or more) infections of a single progenitor cell; similar signal intensity, based on numbers of copies integrated and/or insertion location in the host genome; distinct subcellular localizations of fluorescent proteins. Taken together, these improvements in the complexity of viral infection enable spatial resolution of individual clones.

We performed a careful characterization of this novel cell-tagging reagent *in vitro* before applying it to *in vivo* systems. First, we showed these viruses can label clones in cell culture by introducing serial dilutions of an equal mixture of three viruses (H2B-RFP, Mem-YFP, Mito-CFP) into DF1 cells. As dilution factor increased (Fig. 1C–F), the numbers of double and triple-colored cell clusters decreased logarithmically (Fig. 1G and H); such a pattern was expected if infection with a viral particle is an independent event (Turner and Cepko, 1987). Second, we performed high magnification imaging to confirm the fidelity of the

subcellular localization of distinct fluorescent proteins and excluded the possible effects of optical bleed-through (Fig. 1I–L).

3.2. Clonal relationships within the neural tube

To extend our analysis *in vivo*, we used our recombinant virus to confirm the spatial arrangement of clones in the neural tube. A previous study using time-lapse imaging revealed that these cells undergo oriented division, and in turn, form laterally distributed clusters (Tawk et al., 2007), providing a simple *in vivo* system to validate our reagents. As such, we injected a mixture containing equal amounts of five distinct RIA viruses into the lumen of the neural tube at Hamburger and Hamilton (HH) stage 11 (n = 6), and harvested the embryos 48 h-post infection for imaging thick slices in transverse orientation (Fig. 2A). In a single orthogonal slice, we identified six clones according to the criteria established above; all the clones appeared to align orthogonal to the elongation axis of the neural tube (Fig. 2B and C, Movie S1). We segmented these clones and enclosed them with a polygon using FIJI to measure their Feret's angle, the angle between the maximum diameter of the polygon and the lateral axis of the neural tube (see details in Methods) (Fig. 2D and E). This endpoint analysis revealed an average Feret's angle of about 10°, consistent with the model of lateral clonal expansion suggested by previous longitudinal analyses (Fig. 2F) (Tawk et al., 2007). Both double and triple infection events were rare, with probabilities $p < 0.01$ (Fig. 2G). To rule out the possibility that clonal assessment could be biased if viral aggregates infected adjacent progenitor cells in neural tube, we calculated the error rate of the most frequent doubly infected clone expressing both Mem-YFP and Mito-CFP with the formula previously described (Fields-Berry et al., 1992):

$$\%Error = \frac{no.\ of\ double\ infected\ clone/[2P(C1)P(C2)]}{Total\ clone\ no.}$$

in which, *P(C1)* is the probability of being infected by Mem-YFP virus and *P(C2)* is the probability of being infected with by Mito-CFP virus; both are equal to 1/5 because the same amounts of five viruses were applied. In this particular case, 3 clones with this color combination were identified out of the total 648 clones, leading to an error rate of 5.78% (Fig. 2H), corresponding to a high confidence level in defining clonal boundaries of this combination as well as all other putative clones (Fields-Berry et al., 1992).

Supplementary video related to this article can be found at https://doi.org/10.1016/j.ydbio.2019.03.007.

RIA viruses employed in previous research encoded a single histological marker such as β-galactosidase or alkaline phosphatase, necessitating the need to use highly diluted virus and wide dispersion since individually labeled clones must be separated in order to verify clonality (Fields-Berry et al., 1992). As a result, large number of embryos were required for statistical analysis. In contrast, our multicolor toolkit enables

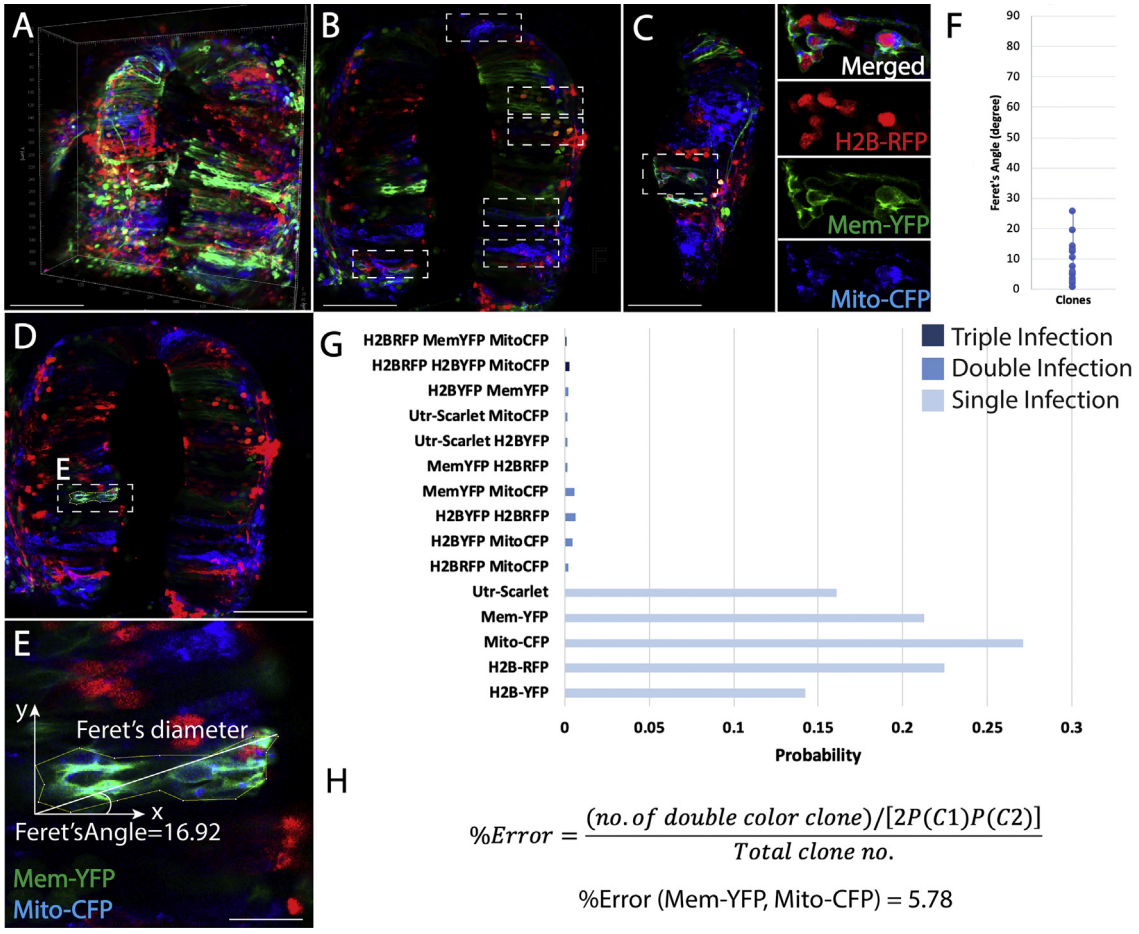

Fig. 2. RIA-mediated multicolor clonal analysis reveals coherent clonal structure in the neural tube. (A) Three-dimensional (3D) view of a chick neural tube infected with viral mixture. (B) In one selected slice of the same tissue in (A), clones (dashed white boxes) appeared to arrange parallelly to the horizontal axis of the tissue. (C) In one representative clone (zoom in view), all the cells expressed three fluorescent proteins in distinct cellular compartments. (D–F) Quantitative analysis reveals lateral distribution of clones. As an example, a double color clone (D) was manually segmented and its Feret's angle was measured (E); in most cases of the 16 clones analyzed, this angle was less than 20° (F). (G) Experimental probability of double and triple-infections are low. (H) Percent error as a result of viral aggregation is about 5.78% for Mem-YFP/Mito-CFP, the most frequent occurring double-infected clone. Scale bars: A-D 100 μm, E 20 μm.

combinatorial tagging and determination of many individual clones within the same tissue preparation, avoiding heterogeneity issues raised from numerous samples and developmental stages.

3.3. Multiplex analysis confirms multipotency of trunk neural crest cells

We next applied this approach to investigate the clonal relationship of cells that migrate extensively and disperse widely throughout the embryo. The trunk neural crest is such an example as it contributes to several tissues along the dorsoventral axis, including dorsal root ganglia (DRG), sympathetic ganglia (SG), and cells along the ventral root (VR) (Bronner-Fraser and Fraser, 1989). The viral mixture described above was introduced into the entire trunk neural tube of chick embryos at Hamburger and Hamilton (HH) stage 11, when trunk neural crest cells are about to emigrate. The embryos were allowed to develop until HH21 (n = 10) when neural crest cells complete migration and begin to differentiate at their final destinations. For live imaging using confocal microscopy, we dissected a thick transverse section (500 μm in thickness) at the forelimb level (Fig. 3A and B) (Li et al., 2019). To capture all the clones within several embryos, we used the tile function of Zeiss LSM 800 to visualize the region from the dorsal neural tube to the dorsal aorta (800 μm × 1600 μm x 150 μm), encompassing most territories through which trunk neural crest cells migrate.

Within individual slices, we observed clonally related cells residing in distinct sites, including the dorsal neural tube (dNT), DRG, SG, and VR (Fig. 3C and DE, double infected clone; FG, triple infected clone). The results suggest that DRG and SG are more clonally associated with each other than with cells along the VR (Fig. 4B). This may be due to the fact that the VR is a smaller tissue, so that cells have less chance to condense within it. Alternatively, cells along the VR may be more developmentally restricted at the time of condensation, or derived from a limited number of progenitor cells.

3.4. Probability calculation confirms the reliability of coinfection-based clonal relationship

Given that many cells with identical color/subcellular localization combinations dispersed across a single embryonic slice at the trunk level (Fig. 4A), we sought to quantitatively verify their clonality. We have demonstrated that in both cell culture and in neural tube (Figs. 1 and 2), infection with multiple viruses is a rare process; the lower the probability of co-infection, the greater the likelihood that cells bearing the same combined color combination are derived from the same precursor. Since migrating neural crest cells are heterogeneous with respect to cell cycle progression and anatomic location, it is challenging to accurately estimate the number of cells infected at time 0. Therefore, we determined the coinfection efficiency by calculating the upper bound of the probability of multiple infection, independent of the initial number of infected progenitor cells. When a given titer of virus is allowed to infect a cell population, each viral particle entering an individual cell can be defined as an independent event. To this end, we estimated the probability of an individual cell being infected with a given number of viruses using a Poisson distribution, which describes discrete events that occur in a fixed time interval and/or space (Figliozzi et al., 2016):

$$P\{n\} = \frac{m^n e^{-m}}{n!}$$

where, P{n} is the probability of infection by n viral particles; m is the multiplicity of infection (MOI), the average number of viral particles per cell. We first measured the titer of the virus to determine the MOI. In a typical experiment, about 0.5 μl of viral mixture with a titer of 1×10^7 pfu/ml per embryo was injected into the trunk segment, suggesting that ~5,000 particles were injected. Next, we estimated the total number of cells in a segment of the neural tube using DAPI. Among these cells, only a portion are premigratory neural crest cells. This is highlighted by expression of the molecular marker Pax7, which marks the premigratory domain (Fig. 4D), though not all Pax7 expressing cells depart from the neural tube. The number of particles that "premigratory" neural crest cells absorb then can be deduced by the total particle number multiplied by the ratio of neural crest to neural tube (approximately 1:5). Taking all these factors into account, the MOI is approximately 0.2 (calculated from an average of 5000 premigratory neural crest cells and 25,000 neural tube cells at the trunk region of interest). The probability of a premigratory neural crest cell in the Pax7 domain being infected with one virus (*P{1}*) is 0.16, with two viruses (*P{2}*) is 0.016, with three viruses (*P{3}*) is 0.001 (Fig. 4C and D). Using the way in which clonality

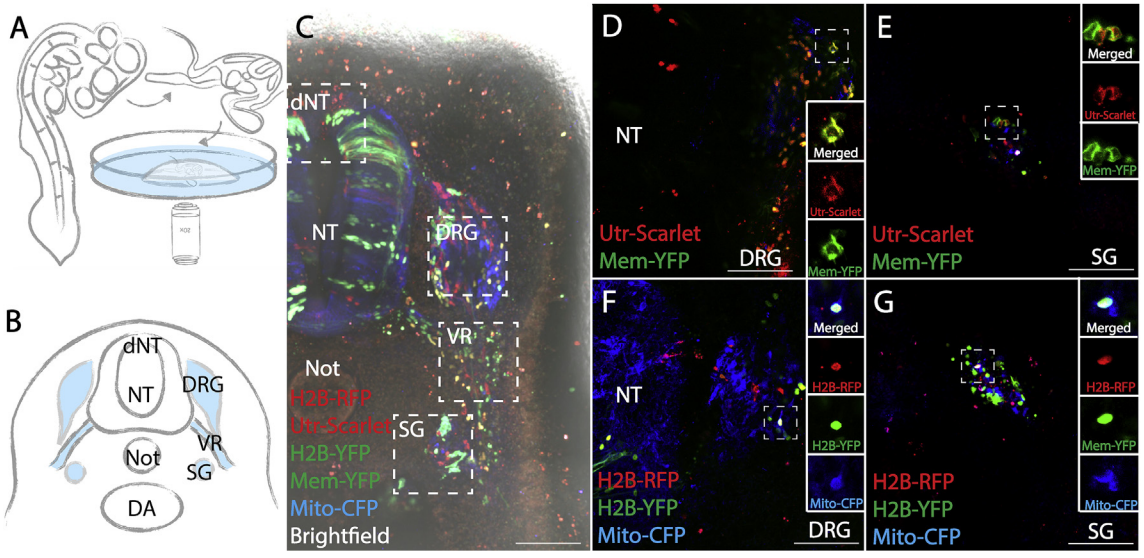

Fig. 3. RIA-mediated multicolor clonal analysis confirms multipotency of trunk neural crest cells. (A) Schematic diagram of experimental procedure. A transverse slice at forelimb level was cut, embedded in 1% agarose for live imaging. (B) Schematic of trunk neural crest derivatives (NT, neural tube; Not, notochord; DA, dorsal aorta; dNT, dorsal neural tube; DRG, dorsal root ganglia; SG, sympathetic ganglia; VR, ventral root; neural crest-derived structures in light blue). (C) A representative transverse view of an infected chick embryo. Regions inside white dashed boxes indicate neural crest-derivatives. (D, E) A double-labeled clone in DRG and SG (Utr-Scarlet, red; Mem-YFP, green) in the same tissue slice. (F, G) A triple-labeled clone in DRG and SG (H2B-RFP, red; H2B-YFP, green; Mito-CFP, blue) in the same tissue slice. Scale bars: C 200 μm; D-G100μm.

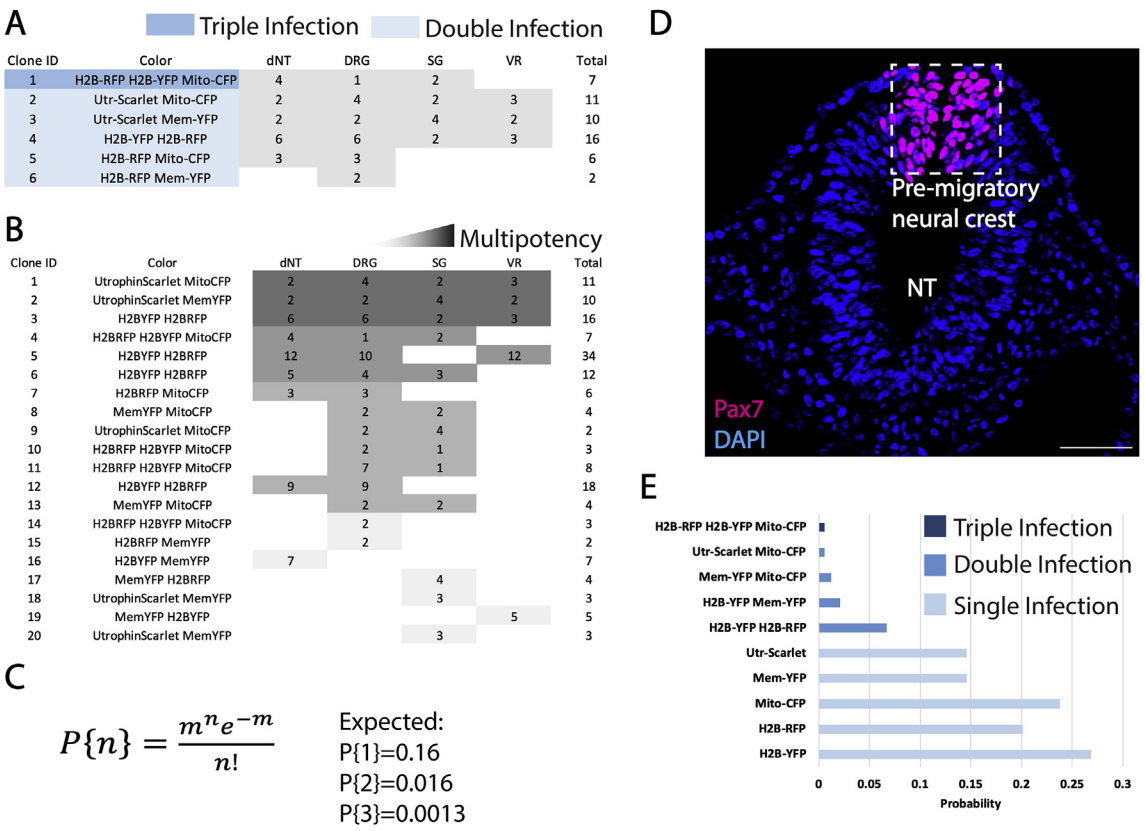

Clone ID	Color	dNT	DRG	SG	VR	Total
1	H2B-RFP H2B-YFP Mito-CFP	4	1	2		7
2	Utr-Scarlet Mito-CFP	2	4	2	3	11
3	Utr-Scarlet Mem-YFP	2	2	4	2	10
4	H2B-YFP H2B-RFP	6	6	2	3	16
5	H2B-RFP Mito-CFP	3	3			6
6	H2B-RFP Mem-YFP		2			2

Clone ID	Color	dNT	DRG	SG	VR	Total
1	UtrophinScarlet MitoCFP	2	4	2	3	11
2	UtrophinScarlet MemYFP	2	2	4	2	10
3	H2BYFP H2BRFP	6	6	2	3	16
4	H2BRFP H2BYFP MitoCFP	4	1	2		7
5	H2BYFP H2BRFP	12	10		12	34
6	H2BYFP H2BRFP	5	4	3		12
7	H2BRFP MitoCFP	3	3			6
8	MemYFP MitoCFP		2	2		4
9	UtrophinScarlet MitoCFP		2	4		2
10	H2BRFP H2BYFP MitoCFP		2	1		3
11	H2BRFP H2BYFP MitoCFP		7	1		8
12	H2BYFP H2BRFP	9	9			18
13	MemYFP MitoCFP		2	2		4
14	H2BRFP H2BYFP MitoCFP		2			3
15	H2BRFP MemYFP		2			2
16	H2BYFP MemYFP	7				7
17	MemYFP H2BRFP			4		4
18	UtrophinScarlet MemYFP			3		3
19	MemYFP H2BYFP				5	5
20	UtrophinScarlet MemYFP			3		3

Fig. 4. Probability calculation of viral co-infection efficiency confirms that double/triple infected clones are rare. (A) An example of clones identified in one embryo. 6/6 of the clones were found in more than one neural crest-derived regions, suggesting multipotency of the progenitor cells. (B) An overview of all the clones identified in multiple embryos (n = 4). 13/20 clones were multipotent. Shade of grey represents the number of places where cells of a particular clone were observed, indicating degree of multipotency. (C) Multiple infection can be portrayed as a Poisson distribution, where the probability of single infection is 0.16, double infection is 0.016, and triple infection is 0.001. (D) Pax7 (Magenta) and DAPI (blue) staining were used to estimate the efficiency of viral infection in (C). (E) Experimentally obtained coinfection index agrees with the theoretical values, demonstrating that double and triple infections are low probability events. Scale bar: 100 μm.

was determined in *Confetti* mouse as a reference (Baggiolini et al., 2015), double and triple infections in our case were rare events. Statistical evaluation under experimental conditions further shows that this probability is close to the theoretical value, despite some variations between *P{1} and P{2}* for different viruses or color combinations. This disparity is possibly due to slight differences in virus titer, or intrinsic variation between the fluorescent protein that affects infection efficiency or expression level, and is also seen in the *Confetti* mouse (Fig. 4E). On this basis, we conclude that cells bearing two to three distinct viral integrations are derived from a single progenitor. Cells bearing similar multiple color combinations can be used as an optical readout of a clone.

Given the fact that RIA viral DNA only integrates into the host genome during metaphase, non-uniform distribution of cell-cycle stages of the infected cells will influence the timing of transgene expression. For cells in metaphase, broken nuclear membrane allows viral integration into the host chromosome; for cells in G1 phase, the viral DNA will stay in the cytoplasm until metaphase; if there are post-mitotic cells in the dorsal neural tube, the viral genes will not express. These factors influence the timing of transgene expression and the estimation of initial viral infection, but also present an opportunity to enhance clonal complexity, as this mosaic context will result in different signal intensity based on the timing of viral DNA integration.

Our result revealing trunk neural crest multipotency is remarkably similar to previous findings based on vital dye injection into individual dorsal neural tube cells in chick (Bronner-Fraser and Fraser, 1989) as well as Wnt1-CreERT and Sox10-Cre ERT driven *R26R-Confetti* mouse (Baggiolini et al., 2015). Whereas dye labeling experiments require single cell injection which is technically challenging and the signal becomes diluted with cell division, viral infection is simple and the fluorescent proteins are stably expressed. Importantly, we can identify multiple clones in a single embryo, as each clone displays a unique color combination resulting from co-infection of two to three viruses (Fig. 3D–G). Compared with *Confetti* system in mice, our approach is significantly more cost-effective and applicable to the chick, the most widely used animal model for neural crest research. Thus, our newly developed RIA-mediated method is an effective albeit much simpler alternative for clonal analysis on dispersed cell populations.

3.5. Combined clonal and cell fate analysis beyond the trunk neural crest

The ultimate goal of lineage analysis is to explore the developmental potential of individual progenitor cells in order to determine their degree of multipotency or lineage restriction. For instance, if neural crest cells acquire their identities early during migration, clonally related cells may express uniform cell fate; alternatively, if cells remain multipotent, and do not commit to a cell fate until they reach the final destination, cells within a clone may disperse and form heterogeneous derivatives. Gaining insights into the latter case requires the ability to examine diverse cell morphologies, localizations, and identities within the same clone. To achieve this goal, lineage tracing needs to be coupled with cell fate analysis.

To test the possibility of combining lineage analysis with cell fate markers, we injected a mixture of viruses in the neural tube adjacent to somites 1–3. Neural crest cells that emerge from this axial level migrate into branchial arches 4 and 6 (Kirby et al., 1983). Embryos were allowed to develop until HH21 and processed for sectioning and immunohistochemistry. Using immunofluorescence, we found that cells labeled with native fluorescent proteins acquired distinct cell fates differentiating into

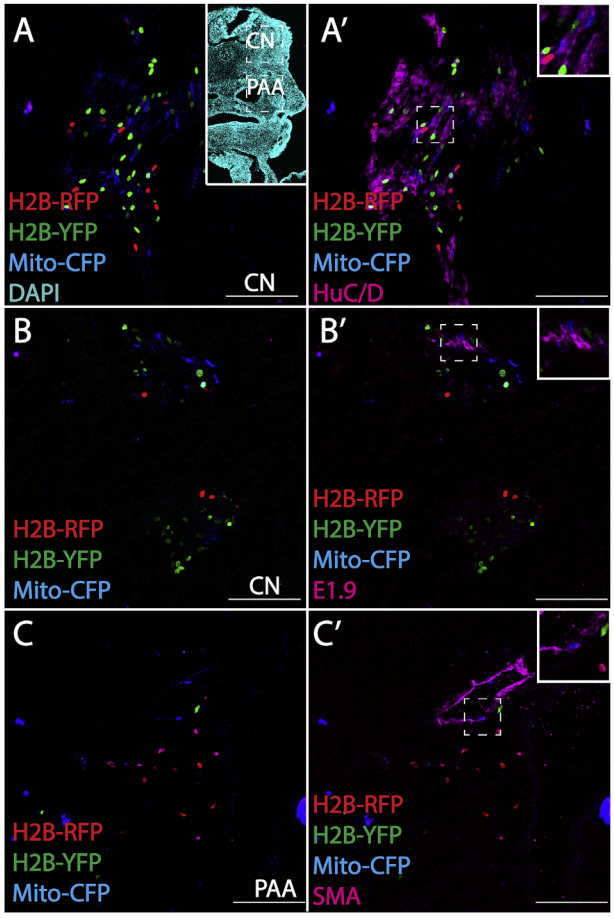

Fig. 5. RIA-mediated clonal analysis can be combined with cell fate studies. A representative transverse section of the virally infected hindbrain was processed for antibody staining. Fluorescently labeled progenies in cranial nerve-IX (CN) and pharyngeal arch arteries (PAA) were indicated with dashed boxes in (A) (DAPI, Cyan). In cranial nerve-IX, neural crest derived cells expressed a neuronal (HuC/D, Magenta) (A, A') or sensory/motor neuron marker (E1.9, Magenta) (B, B'); some of their siblings can migrate more ventrally into the pharyngeal arch arteries (PAA) and differentiated into smooth muscle (SMA, Magenta) (C, C'). Scale bars: 100 μm.

neurons (HuC/D, Fig. 5A, A'), including primary sensory or motor neuron (E1.9, Fig. 5B, B'), as well as smooth muscle (SMA, Fig. 5C, C'). Taken together, our results show that RIA-mediated lineage analysis is compatible with post-processing such as paraformaldehyde fixation, cryo-sectioning and antibody staining, while the endogenous fluorescence signal is well-preserved.

4. Conclusion

In summary, by modifying RIA viruses to enable simultaneous expression of different fluorophores, we present a useful means to orthogonally detect multiple clones in single avian embryos. We demonstrate the utility of this approach in cell culture, the neural tube and neural crest. Our results on migrating neural crest cells confirm the multipotency of this cell population that has been demonstrated previously by other complementary techniques (Bronner-Fraser and Fraser, 1988; Baggiolini et al., 2015). Moreover, our RIA virus constructs are designed to enable co-expression of fluorophores and proteins that function either normally or as mutants (Gandhi et al., 2017; Li et al., 2017) for the purpose of gene perturbation experiments or time-lapse imaging (Li et al., 2015) at clonal level. This approach simplifies clonal analysis in avian embryos and broadens the range of cell types to which cell lineage analysis can be applied.

Author contributions

W.T., Y.L. and M.E.B conceived the project. W.T., Y.L. and S.G performed the experiments. W.T., Y.L. and M.E.B wrote the paper with consultation from S.G.

Funding

This work is supported by NIHR01DE027568 and NIHRO1HL14058 to M.E.B and American Heart Association predoctoral fellowship 18PRE34050063 to S.G.

Conflicts of interest

The authors declare no competing interests.

Acknowledgement

We thank Alison Koontz for providing insightful suggestions on probability calculation, Can Li, Felipe Vieceli, David Miller for technical support. We thank Carlos Lois laboratory and Caltech Biological Imaging Facility for sharing equipment.

References

Ayer-Le Lievre, C.S., Le Douarin, N.M., 1982. The early development of cranial sensory ganglia and the potentialities of their component cells studied in quail-chick chimeras. Dev. Biol. 94 (2), 291–310. Retrieved from. http://www.ncbi.nlm.nih.gov/pubmed/7152108.

Baggiolini, A., Varum, S., Mateos, J.M., Bettosini, D., John, N., Bonalli, M., et al., 2015. Premigratory and migratory neural crest cells are multipotent in vivo. Cell Stem Cell 16 (3), 314–322. https://doi.org/10.1016/j.stem.2015.02.017.

Bénazéraf, B., Francois, P., Baker, R.E., Denans, N., Little, C.D., Pourquié, O., 2010. A random cell motility gradient downstream of FGF controls elongation of an amniote embryo. Nature 466 (7303), 248–252.

Bronner-Fraser, M., Fraser, S., 1989. Developmental potential of avian trunk neural crest cells in situ. Neuron 3 (6), 755–766. Retrieved from. http://www.ncbi.nlm.nih.gov/pubmed/2484346.

Bronner-Fraser, M., Fraser, S.E., 1988. Cell lineage analysis reveals multipotency of some avian neural crest cells. Nature 335 (6186), 161–164. https://doi.org/10.1038/335161a0.

Cai, D., Cohen, K.B., Luo, T., Lichtman, J.W., Sanes, J.R., 2013. Improved tools for the Brainbow toolbox. Nat. Methods 10 (6), 540–547. Retrieved from. http://www.ncbi.nlm.nih.gov/pubmed/23866336.

Chen, C., Smith, D., Peters, M., Samson, M., Zitz, J., Tabin, C., Cepko, C., 1999. Production and design of more effective avian replication-incompetent retroviral vectors. Dev. Biol. 214 (2), 370–384.

Fields-Berry, S.C., Halliday, A.L., Cepko, C., 1992. A recombinant retrovirus encoding alkaline phosphatase confirms clonal boundary assignment in lineage analysis of murine retina. Proc. Natl. Acad. Sci. Unit. States Am. 89, 693–697.

Figliozzi, R.W., Chen, F., Chi, A., Hsia, S.-C.V., 2016. Using the inverse Poisson distribution to calculate multiplicity of infection and viral replication by a high-throughput fluorescent imaging system. Virol. Sin. 31 (2), 180–183. https://doi.org/10.1007/s12250-015-3662-8.

Frank, E., Sanes, J.R., 1991. Lineage of neurons and glia in chick dorsal root ganglia: analysis in vivo with a recombinant retrovirus. Development (Cambridge, England) 111 (4), 895–908. Retrieved from. http://www.ncbi.nlm.nih.gov/pubmed/1908772.

Gandhi, S., Piacentino, M.L., Vieceli, F.M., Bronner, M.E., 2017. Optimization of CRISPR/Cas9 Genome Editing for Loss-Of-Function in the Early Chick Embryo. Dev Biol. 432 (1), 86–97.

Gerrits, A., Dykstra, B., Kalmykowa, O.J., Klauke, K., Verovskaya, E., Broekhuis, de Haan, G., Bystrykh, L.V., 2010. Cellular barcoding tool for clonal analysis in the hematopoietic system. Blood 115 (13), 2610–2618. https://doi.org/10.1182/blood-2009-06-229757.

Kirby, M.L., Gale, T.F., Stewart, D.E., 1983. Neural crest cells contribute to normal aorticopulmonary septation. Science (New York, N.Y.) 220 (4601), 1059–1061. Retrieved from. http://www.ncbi.nlm.nih.gov/pubmed/6844926.

Krispin, S., Nitzan, E., Kassem, Y., Kalcheim, C., 2010. Evidence for a dynamic spatiotemporal fate map and early fate restrictions of premigratory avian neural crest. Development (Cambridge, England) 137 (4), 585–595. https://doi.org/10.1242/dev.041509.

Lewis, A.E., Vasudevan, H.N., O'Neill, A.K., Soriano, P., Bush, J.O., 2013. The widely used Wnt1-Cre transgene causes developmental phenotypes by ectopic activation of Wnt signaling. Dev. Biol. 379 (2), 229–234. https://doi.org/10.1016/j.ydbio.2013.04.026.

Li, Y., Trivedi, V., Truong, T.V., Koos, D.S., Lansford, R., Chuong, C.M., Warburton, D., Moats, R.A., Fraser, S.E., 2015. Dynamic imaging of the growth plate cartilage reveals

multiple contributors to skeletal morphogenesis. Nat. Commun. 6, 6798. https://doi.org/10.1038/ncomms7798.

Li, Y., Li, A., Junge, J., Bronner, M., 2017. Planar cell polarity signaling coordinates oriented cell division and cell rearrangement in clonally expanding growth plate cartilage. ELife 6, e23279. https://doi.org/10.7554/eLife.23279.

Li, Y., Junge, J.A., Miner, J.H., Arnold, D.B., Fraser, S.E., 2018. Discs large 1 controls daughter cell polarity after cytokinesis during skeletal formation. Proc. Natl. Acad. Sci. Unit. States Am. 115 (46), E10859–E10868, 1713959115.

Li, Y., Vieceli, F.M., Gonzalez, W.G., Li, A., Tang, W., Lois, C., Bronner, M.E., 2019. In vivo quantitative imaging provides insights into trunk neural crest migration. Cell Rep. 26 (6), 1489–1500 e3. https://doi.org/10.1016/j.celrep.2019.01.039.

Livet, J., Weissman, T.A., Kang, H., Draft, R.W., Lu, J., Bennis, R.A., Sanes, J.R., Lichtman, J.W., 2007. Transgenic strategies for combinatorial expression of fluorescent proteins in the nervous system. Nature 450 (7166), 56–62. https://doi.org/10.1038/nature06293.

Pearse, R.V., Scherz, P.J., Campbell, J.K., Tabin, C.J., 2007. A cellular lineage analysis of the chick limb bud. Dev. Biol. 310 (2), 388–400. https://doi.org/10.1016/j.ydbio.2007.08.002.

Sanes, J.R., 1989. Analysing cell lineage with a recombinant retrovirus. Trends Neurosci. 12 (1), 21–28. Retrieved from. http://www.ncbi.nlm.nih.gov/pubmed/24713.

Sulston, J.E., 1983. Neuronal cell lineages in the nematode Caenorhabditis elegans. Cold Spring Harbor Symp. Quant. Biol. 48 (Pt 2), 443–452. https://doi.org/10.1101/SQB.1983.048.01.049.

Tawk, M., Araya, C., Lyons, D.A., Reugels, A.M., Girdler, G.C., Bayley, P.R., Hyde, D.R., Tada, M., Clarke, J.D.W., 2007. A mirror-symmetric cell division that orchestrates neuroepithelial morphogenesis. Nature 446 (7137), 797–800. https://doi.org/10.1038/nature05722.

Turner, D.L., Cepko, C.L., 1987. A common progenitor for neurona and glia persists in rat retina late in development. Nature 328, 131–136.

Weston, J.A., Thiery, J.P., 2015. Pentimento: neural crest and the origin of mesectoderm. Dev. Biol. 401 (1), 37–61. https://doi.org/10.1016/j.ydbio.2014.12.035.